

# Atomic Vacancies Control of Pd-Based Catalysts for Enhanced Electrochemical Performance

Yunpeng Zuo, Dewei Rao, Shuo Li, Tingting Li, Guilin Zhu, Shuangming Chen, Li Song, Yang Chai,\* and Heyou Han\*

Structure-engineered Pd-based catalysts at the atomic level can effectively improve the catalytic performance for oxygen or small organic molecules electrocatalysis, comparable to or even superior to that of commercial Pt/C. Here, PdCuCo anisotropic structure (AS) electrocatalysts are synthesized with abundant vacancy defects on the exterior surface, which is unambiguously verified by aberration-corrected transmission electron microscopy. The PdCuCo-AS with vacancy (v-PdCuCo-AS) shows excellent electrochemical activity toward oxygen reduction (ORR) and oxidation of alcohols. The mass activity of the v-PdCuCo-AS is 0.18 A mg<sup>-1</sup> at 0.9 V versus reversible hydrogen electrode (RHE), which is 15.55 times larger than that of the commercial Pd/C catalyst in acidic electrolyte. According to the theoretical calculations, this significant improvement can be understood as a result of the promoted charge transfer by polarized electronic structures of the v-PdCuCo-AS in the processes of ORR. The synergistic effect of the correlated defects and the compressive strain caused by the doping Co and Cu atoms effectively improve the electrocatalysis activity for the ORR in acidic/alkaline electrolyte on the v-PdCuCo-AS stems. This approach provides a strategy to design other AS structures for improving their electrochemical performance.

difficult to obtain the catalysts without defects.<sup>[4]</sup> Some studies have demonstrated that the catalysts with defects on the surface possess higher activity than the defect-free ones.<sup>[4,14–16]</sup> For instance, it has been proved that the activity of the edge carbon is higher than basal plane carbon for the ORR.<sup>[17]</sup> Meanwhile, S-vacancies in the basal plane of MoS<sub>2</sub> provide more exposed Mo atoms to directly bind with hydrogen.<sup>[18]</sup> The catalysts with controllable defects have great potential for high activity and the commercialization of the noble metal catalysts.

Fuel cells are high-efficiency energy-conversion devices.<sup>[19–23]</sup> The best currently known electrocatalysts for ORR and liquid fuels-oxidation reaction are the Pt-based catalysts, which suffers from high cost, undesirable durability, and low CO poisoning tolerance problems.<sup>[23]</sup> Recently, Pd-based catalysts have been demonstrated to be promising effective catalysts because of their outstanding activities

Controlling the exterior surface structure of the electrode materials can be used to enhance the activity of catalyst, which has been widely applied for the sustainable conversion processes of water-hydrogen-oxygen, including the oxygen reduction reaction (ORR), oxygen evolution reaction, and hydrogen evolution reaction (HER).<sup>[1–5]</sup> The configuration of surface electronic structure is closely related to the arrangement of surface atoms of the materials.<sup>[6–9]</sup> However, most current systems only focus on the structures, sizes, or components, neglecting the effect of the intrinsic defects of the crystals.<sup>[1,10–13]</sup> In fact, it is quite

for ORR and electrochemical oxidation of small organic molecules, which show potential alternatives for the Pt-based catalysts.<sup>[13,24–26]</sup> Previous studies show appreciable enhancement of the activity of the catalysts in water splitting and fuel cells by alloying Pd with the transition metals, exposing the low-coordinated surface atoms, and altering the distances between surface atoms to control the defect or strain of catalysts.<sup>[13,26–28]</sup> A range of transition metals, including Fe, Co, and Ni, have been intensively explored into PdCu active bimetallic system by simultaneously decreasing material cost and enhancing


Y. Zuo, S. Li, G. Zhu, Prof. H. Han  
State Key Laboratory of Agricultural Microbiology  
College of Science  
Huazhong Agricultural University  
Wuhan 430070, P. R. China  
E-mail: hyhan@mail.hzau.edu.cn

Y. Zuo, Prof. Y. Chai  
Department of Applied Physics  
The Hong Kong Polytechnic University  
Hung Hom, Kowloon 999077, Hong Kong, P. R. China  
E-mail: ychai@polyu.edu.hk

Dr. D. Rao  
School of Materials Science and Engineering  
Jiangsu University  
Zhenjiang 212013, P. R. China

Dr. T. Li  
Key Laboratory of Micro-Nano Materials for Energy Storage  
and Conversion of Henan Province  
Institute of Surface Micro and Nano Materials  
Xuchang University  
Xuchang, Henan 461002, P. R. China

Dr. S. Chen, Prof. L. Song  
National Synchrotron Radiation Laboratory  
CAS Center for Excellence in Nanoscience  
University of Science and Technology of China  
Hefei, Anhui 230029, P. R. China

 The ORCID identification number(s) for the author(s) of this article can be found under <https://doi.org/10.1002/adma.201704171>.

DOI: 10.1002/adma.201704171

performance.<sup>[4,22,23]</sup> The specific activity (SA) for ORR of the ordered PdCuCo nanoparticles can reach 1.3 times higher than that of commercial Pt/C with the compressive strain on the surface of the catalysts.<sup>[13]</sup> Huang and his co-workers found that the ascorbic acid not only acts as the reductant but also works as the weak acid to remove the heteroatoms, forming the pure Pt phase on the surface of the crystals.<sup>[29]</sup> Thus the heteroatoms can be synchronously and selectively removed in the reaction to obtain the catalysts with abundant defects. Stimulated by this, considerable efforts have been made to develop the PdCuCo catalysts with abundant vacancies (v-PdCuCo) toward oxygen electrocatalysis.

In this work, we show a general method with high reproducibility for controllable synthesis of a class of multicomponent anisotropic structure (AS) with abundant active defect sites. The open AS addresses large specific surface area, 3D surface molecular accessibility, and high densities of corners, edges, and stepped atoms, which can optimize the use of noble metals.<sup>[6,30,31]</sup> The structural characterization analysis was obtained by aberration corrected high-resolution transmission electron microscopy (HRTEM), indicating the existence of atomic vacancies. The anisotropic materials can achieve high surface-to-volume ratio even though there is an accumulation of the carbon-supported catalyst. Our density functional theory (DFT) calculations reveal that the vacancies enable the polarization of surface electronic structure for v-PdCuCo-AS, which can improve the ORR activities of the v-PdCuCo-AS. Moreover, upscaled synthesis of v-PdCuCo-AS can be readily achieved at gram scale, and the approach is an effective strategy to design other AS systems.

The structures of as-prepared v-PdCuCo-AS are characterized by aberration-corrected transmission electron microscopy (AC-TEM). **Figure 1A** shows representative high-angle annular dark field (HAADF) images of v-PdCuCo-AS. The geometry of multihierarchical structure (Figure 1A and Figure S1, Supporting Information) with the branch diameter of  $\approx 9$  nm is observed, which can help the molecular to contact with catalysts.<sup>[6,30]</sup> The selected-area electron diffraction (SAED) of the as-prepared nanomaterials (inset of Figure 1A) shows the v-PdCuCo-AS is single crystalline, with the corresponding diffraction pattern from the [02-2] zone axis of PdCu cubic phase.<sup>[13,32,33]</sup> The obvious contrast between the vacancies sites and bulk atoms can be attributed to the ingredients in the v-PdCuCo-AS. A typical area of v-PdCuCo-AS image (Figure 1B) was selected to observe the dispersed vacancies sites. The enlarged HRTEM images show the atomic structure of v-PdCuCo-AS with the [110] direction in the zone axis. As a rigorous technique to document the element distribution of the nanomaterials, scanning TEM-energy dispersive spectrometer (STEM-EDS) elemental mapping of the individual v-PdCuCo-AS shows that Co is homogeneously distributed in the interior area of the catalyst, whereas Pd and Cu were distributed throughout the v-PdCuCo-AS structure (Figure 1C and Figure S2, Supporting Information). The outer heteroatoms might be etched by ascorbic acid owing to the weak acid.<sup>[29]</sup> The HRTEM images of v-PdCuCo-AS clearly show the vacancies sites are uniformly distributed around the catalysts (Figure 1B1 and **Figure 2**). The higher magnification HRTEM and the inset HAADF images in Figures 1B1 and 2 indicated the vacancies, which can be identified from their different contrast as the red

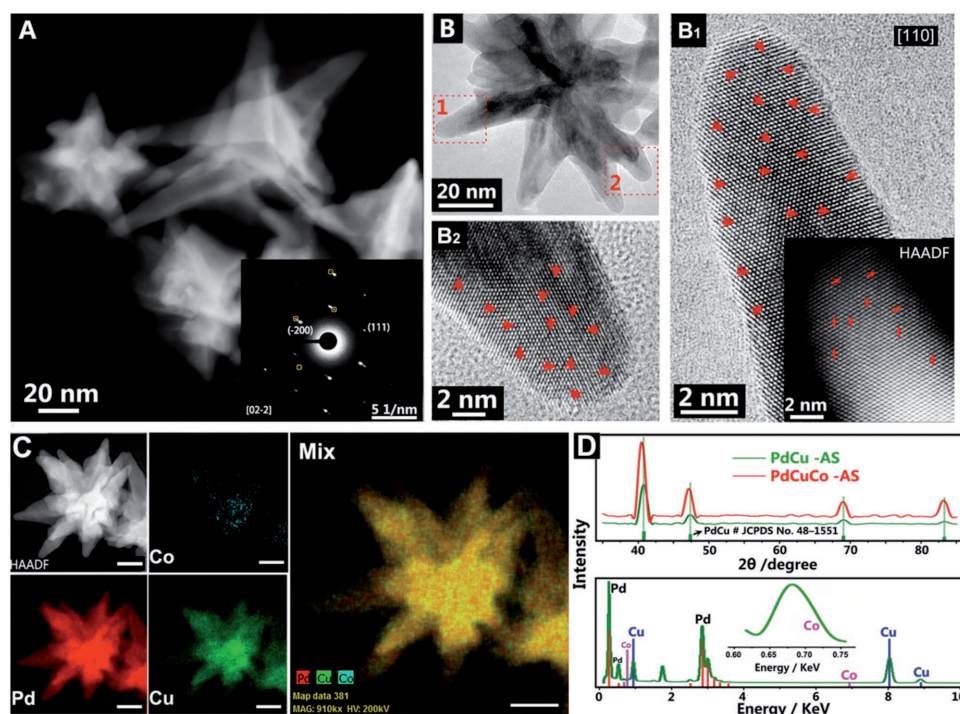


**Figure 1.** Representative A) HAADF-STEM (HS) image and the inset is SAED image. B,B<sub>1,2</sub>) HRTEM images projected along the zone axes of [110] axis and the corresponding bright-field image of a dendritic structure. C) The typical HS image and the rests are the corresponding STEM-EDS elemental mapping of an individual v-PdCuCo-AS. D) XRD patterns and TEM-EDX of v-PdCuCo-AS. Scale bars are 20 nm in (C).

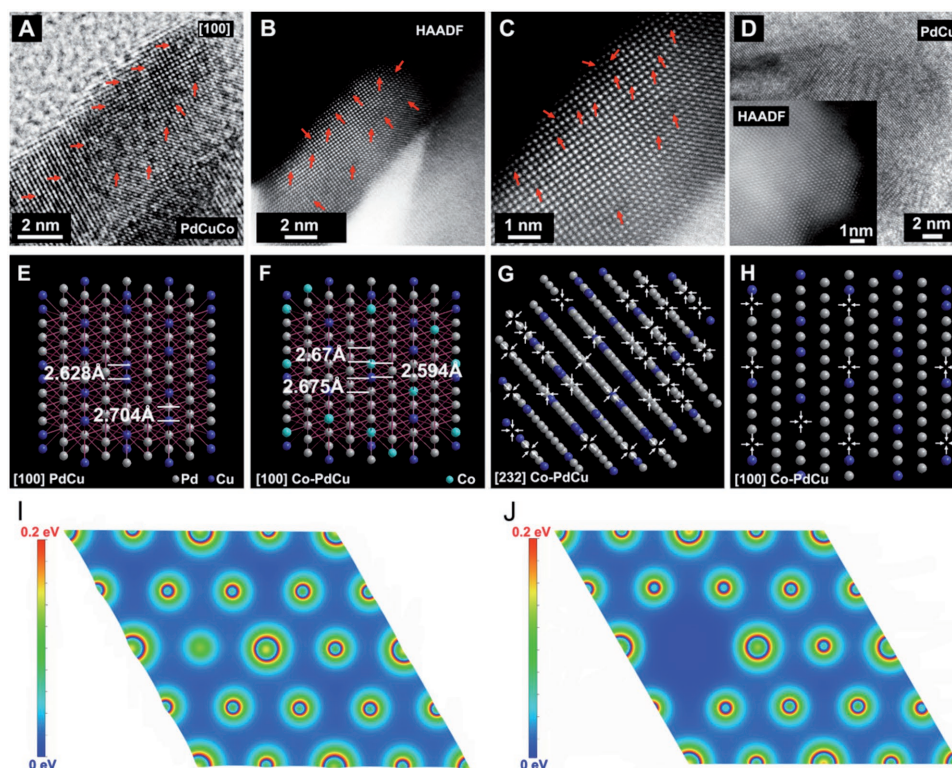


**Figure 2.** A) HRTEM image of a typical branch of the PdCu-Co-AS from the [100] direction. B,C) The corresponding enlarged HAADF images. D) HRTEM image of a typical branch of the PdCu-AS. The inset is the corresponding HRTEM image. E,F) The approximate PdCu-AS/v-PdCuCo-AS crystal structure from [100] with Pd in grayness, Cu in blue, and Co in soft blue and G,H) the hollow defect sites of the v-PdCuCo-AS from [232] and [100] perspectives of the crystal structure. I) The surface charge density of the Co embedded PdCu-AS and J) the vacancy in v-PdCuCo-AS.

arrows indicate. These results are further supported by the X-ray diffraction (XRD) and STEM-EDS. It is noteworthy that there are no typical diffraction peaks of Cu or its oxides, and the peaks are in the central area between the fcc Pd and Cu, indicating the formation of PdCu alloy.<sup>[13,32,33]</sup> From the XRD spectrum (Figure 1D), the diffraction peaks can be well identified to the (111), (200), (220), and (311) for the fcc PdCu-AS with the Joint Committee on Powder Diffraction Standards (JCPDS) number: 48-1551. The XRD pattern of v-PdCuCo-AS significantly shifts to low angle X-ray diffraction area owing to the increased lattice spacing by imbedding Co atoms.<sup>[34,35]</sup>

Surface analysis of the v-PdCuCo-AS was carried out using X-ray photoelectron spectroscopy (XPS) technique (Figure S3, Supporting Information). The XPS spectroscopy shows the presence of Pd, Cu, and Co in the catalyst. The presence of the blurry Co peak in the full spectrum (Figure S3A, Supporting Information) and the enlarged single unsharp Co2p peak in Figure S3B in the Supporting Information reveal that the surface Co atoms were leached away from the PdCuCo catalysts,<sup>[36–38]</sup> in consistent with the STEM EDS-mapping-based study of v-PdCuCo-AS catalysts. The X-ray absorption near edge structure and extended X-ray absorption fine structure in Figure S4 in the Supporting Information show negligible change of Cu for the PdCu-AS and v-PdCuCo-AS catalysts, which reveal the vacancy defects on the surface of the v-PdCuCo-AS are caused by removing of Co atoms as mentioned before. The compositional ratio between Pd/Cu/Co is 3.87/1/0.01 for

the v-PdCuCo-AS, as revealed by inductively coupled plasma mass spectrometry (ICP-MS) documented in Table S1 in the Supporting Information. The ICP-MS results confirmed the low Co content as revealed by STEM-EDS mapping. The vacant sites might be influenced by the use of ascorbic acid, which can act as a weak acid for removing the heteroatoms, allowing the abundant vacancies sites to diffuse on the exterior surface of the v-PdCuCo-AS.<sup>[29,37]</sup>

We can observe that abundant vacancies sites with randomly scattered distribution over the surface through the HRTEM image obtained from the [100] axis in Figure 2A. The corresponding HAADF images in the Figure 2B,C reveal that the defective regions (pointed out by the red arrow) mainly exist on the surface of the v-PdCuCo-AS structure, which provide further evidence for the results shown in Figure 1. For the fcc PdCu nanocrystals, the atomic arrangement forms alternating packing of Pd and Cu atoms along the <100> direction. While for the v-PdCuCo-AS, the Co atoms possibly cause the polar facets owing to embedded configuration and the intrinsic physical property. There is a significant difference of the arrangement of the crystal structure between the PdCu-AS and v-PdCuCo-AS (comparing the Figure 2A,B with Figure 2D and Figure S5, Supporting Information). Figure 2E,F shows the approximate PdCu and v-PdCuCo-AS crystal structures along the [100] direction with Pd in grayness, where Cu is in blue and Co is in soft blue. For the PdCu-AS, the adjacent Pd–Cu and Cu–Cu atom–atom distances are 2.704 and 2.628 Å (Figure 2E);

however, the adjacent Cu–Pd atom–atom distance decreases to 2.675 Å with the increase of Cu–Pd atom–atom distance after embedded Co atoms to the PdCu crystal. To further identify the atomic arrangement of the surface structure, the approximate v-PdCuCo-AS crystal structure from [232] and [100] perspectives (Figure 2G,H) are helpful for understanding the distinction of the different metal atoms in the bulk catalyst. The vacancies on the surface possess slightly larger atomic distances than the inner Pd atoms do, which provides spatial locations for strain release.<sup>[39]</sup> The approximate v-PdCuCo-AS crystal structures in Figure 2G,H show that the coordination number of the surface atoms are undercoordinated relative to typical crystal surfaces.<sup>[40]</sup> For the PdCuCo catalyst, the surface charge density at site of Co is changed as the formation of vacancy (Figure 2I,J and Figure S6, Supporting Information). It is noteworthy that the introduction of Co can also increase the electronic polarization of the PdCu-AS (Figure 2I and Figure S6, Supporting Information), which helps to overcome the reaction barrier of the limiting steps of ORR, thus improving ORR activity.<sup>[41]</sup>

The formation process of v-PdCuCo-AS contains nucleation and growth steps.<sup>[9,22]</sup> The hexadecyl trimethyl ammonium bromide (CTAB) molecules and Br<sup>-</sup> act as the capping agents, which have great effect on the final structure of the v-PdCuCo-AS materials.<sup>[42]</sup> The metal atoms agglomerate to form nanoclusters, which subsequently grow to small PdCuCo particles (Figure S7A,B, Supporting Information) after the content of corresponding atoms reached the level of supersaturation.<sup>[42]</sup> The formation of small PdCuCo particles may abide by the law of Wulff's theorem, attempting to minimize the total interfacial free energy ( $\gamma$ ) of the system.<sup>[43–47]</sup> This result is consistent with

the previously reported papers on the shape evolution of the nanocrystals.<sup>[42–47]</sup> The reaction progress of PdCuCo truncated nanocubic generated from the PdCuCo particles is shown in Figure S7A,C in the Supporting Information. The new generated zero-valent metal atoms deposit onto the special active sites as the CTAB molecules and Br<sup>-</sup> absorb on the {100} facets, which have remarkable influence on the surface energy.<sup>[9,43–47]</sup> The differentiation of the interfacial energy for the intermediates accelerates the island growth to form the anisotropic structures, as shown in Figure S7A,D in the Supporting Information. There are abundant steps, corners on the surface of the catalyst in the formation of the branches, which comprise the high-index facets {310}, {420} in the inset HRTEM images (Figure S7A, Supporting Information). According to enlarged HRTEM images in Figure S7A in the Supporting Information, the lattice spacing of the architecture is estimated to be 0.22 nm (Figure S7A, Supporting Information), consistent with the {111} facets of *fcc* PdCuCo crystal, confirming the growth of PdCuCo branch at <111> direction and the existence of PdCuCo nanocubics. After the PdCuCo-AS generation, the composites continue to stir for a period of time to leach away the Co or Cu atoms on the surface to generate the vacancies sites for the v-PdCuCo-AS.

The electrochemical performance of the PdCu-AS and v-PdCuCo-AS toward ORR were evaluated in O<sub>2</sub>-saturated 0.1 M HClO<sub>4</sub> solution against the commercial Pd/C (20% Pd, JM) (Figure 3). The electrochemical surface area (ECSA) of the catalysts was determined by integrating the hydrogen adsorption charge on cyclic voltammograms (CVs), as shown in Figure 3A. The characteristic region of Hupd (H<sup>+</sup> + e<sup>-</sup> =

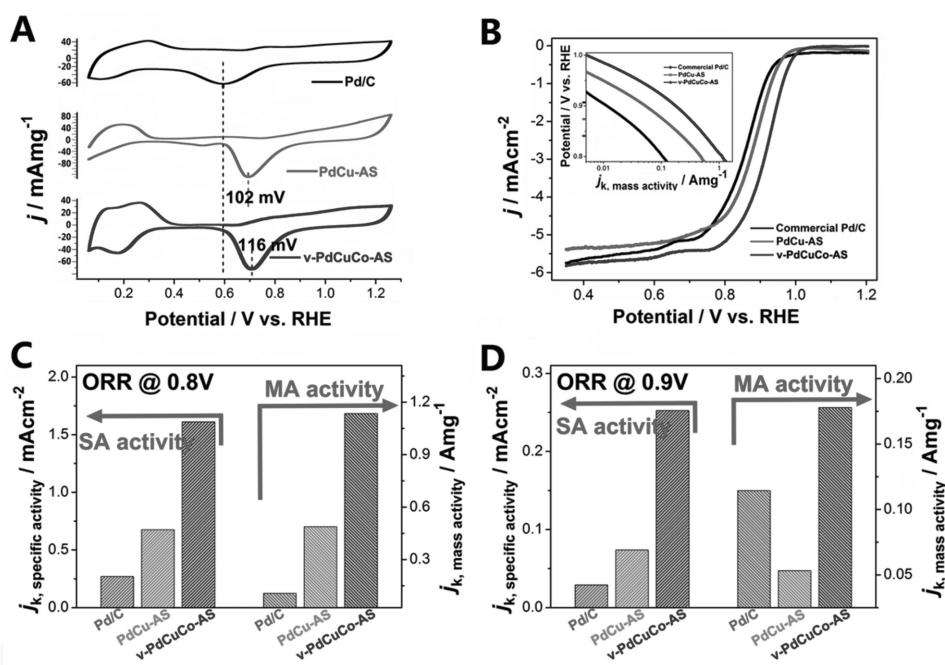


**Figure 3.** Electrocatalytic properties of commercial Pd/C, PdCu-AS, and v-PdCuCo-AS catalysts. A) The CVs of the catalysts tested in 0.1 M HClO<sub>4</sub> solution at room temperature with the sweep rate of 50 mV s<sup>-1</sup>. B) The ORR polarization curves were recorded in O<sub>2</sub>-saturated 0.1 M HClO<sub>4</sub> and the inset was the corresponding mass activity Tafel plots for the three catalysts, respectively. Comparison of specific activities and mass activities of the Pd/C, PdCu-AS, and v-PdCuCo-AS catalysts at C) 0.8 V versus RHE and D) 0.9 V versus RHE, showing that the v-PdCuCo-AS deliver the enhanced ORR performance of the Pd/C and PdCu-AS catalysts.

Hupd) adsorption/desorption for the Pd/C, PdCu-AS, and v-PdCuCo-AS is in the potential range from 0.05 to 0.4 V. The reduction of Pd oxide for the OHad ( $2\text{H}_2\text{O} = \text{OHad} + \text{H}_3\text{O}^+ + e^-$ ) is in the potential between 0.65 and 1.25 V. The ECSA/ $g_{\text{Pd}}$  of the Pd/C, PdCu-AS, and v-PdCuCo-AS are 41.79, 72.18, and  $70.46 \text{ m}^2 \text{ g}^{-1}$ , respectively. That is mainly because the AS can offer the 3D surface molecular accessibility.<sup>[6]</sup> The reduction potential of surface oxides of the PdCu-AS and v-PdCuCo-AS shift positively by 102 and 116 mV compared to Pd/C, revealing the decrease in oxygen affinity of the PdCu-AS and v-PdCuCo-AS.<sup>[48]</sup> The ORR polarization curves normalized with respect to the area of glassy carbon electrode (GCE,  $0.196 \text{ cm}^2$ ) are presented in Figure 3B. The half-wave potential for v-PdCuCo-AS is 0.915 V versus reversible hydrogen electrode (RHE), which is obviously higher than that of the commercial Pd/C (0.856 V vs RHE) and PdCu-AS (0.88 V vs RHE) as shown in Figure 3B, suggesting significantly enhanced ORR activity for v-PdCuCo-AS catalyst.<sup>[40]</sup> The kinetic currents are calculated in accordance with the Koutecky–Levich equation.<sup>[40,41,49–51]</sup> As seen from the corresponding Tafel plots in Figure 3B, v-PdCuCo-AS exhibits significantly improved kinetics with a smaller slope compared with PdCu-AS, revealing that the randomly distributed defective sites can effectively improve the activity of the v-PdCuCo-AS.<sup>[40,41,48]</sup> To better assess the ORR activity, we also analyze the corresponding SA and mass activity (MA) of synthetic catalysts at 0.8 and 0.9 V versus RHE. Overall, as expected, the SA of v-PdCuCo-AS catalyst at 0.8 V versus RHE could reach  $1.61 \text{ mA cm}^{-2}$ , 2.4 times the SA of PdCu-AS ( $0.675 \text{ mA cm}^{-2}$ ) and 5.96 times the SA of Pd/C ( $0.27 \text{ mA cm}^{-2}$ ) (Figure 3C). The MA of v-PdCuCo-AS catalyst at 0.8 V versus RHE is  $1.135 \text{ A mg}^{-1}$ , 10.67 and 2.33 times greater than those of the Pd/C ( $0.106 \text{ A mg}^{-1}$ ) and PdCu-AS ( $0.487 \text{ A mg}^{-1}$ ), respectively. Simultaneously, the SA of v-PdCuCo-AS catalyst at 0.9 V versus RHE was  $0.252 \text{ mA cm}^{-2}$ , 3.42 times the SA of PdCu-AS ( $0.074 \text{ mA cm}^{-2}$ ) and 8.69 times of Pd/C ( $0.029 \text{ mA cm}^{-2}$ ) (Figure 3D), respectively. The MA of v-PdCuCo-AS catalyst at 0.9 V versus RHE is  $0.178 \text{ A mg}^{-1}$ , 15.55 times the MA of the Pd/C ( $0.011 \text{ A mg}^{-1}$ ) and 3.34 times the MA of the PdCu-AS ( $0.053 \text{ A mg}^{-1}$ ), respectively. In addition, the electrocatalysis activity of commercial Pt/C was also tested to compare the performance with the v-PdCuCo-AS. The MA of the Pt/C at 0.9 V versus RHE ( $0.1495 \text{ A mg}^{-1}$ , Figure S8, Supporting Information) is smaller than that of v-PdCuCo-AS ( $0.178 \text{ A mg}^{-1}$ ), which shows good catalytic performance of v-PdCuCo-AS. These results and the comparisons to Pd-based catalysts from recent studies in Table S3 in the Supporting Information suggest an excellent structure and composition of the synthetic v-PdCuCo-AS. We also synthesized PdCuCo nanomaterials with different sizes, which contains the PdCuCo-AS (37, 41, and 52 nm) and PdCuCo nanoparticles (22 nm), as shown in Figure S9 in the Supporting Information. When the whole size of the dendritic structure increased to 52 nm, the extension of the branched protuberance also increases (Figure S9, Supporting Information). The ORR polarization curves show that the catalytic activity of the PdCuCo-AS gradually increase as the branched protuberance gets larger (Figure S9, Supporting Information). As shown in Figure S10 in the Supporting Information, the MA of PdCuCo nanocrystal with the size of 52 nm at 0.8 V versus RHE is  $0.281 \text{ A mg}^{-1}$ , which is greater

than those of the PdCuCo (22 nm,  $0.102 \text{ A mg}^{-1}$ ), PdCuCo (37 nm,  $0.040 \text{ A mg}^{-1}$ ), and PdCuCo (41 nm,  $0.232 \text{ A mg}^{-1}$ ), respectively. This trend is mainly because the branches in the PdCuCo-AS can adequately expose the active sites with the high densities of edges, corners, and stepped atoms.<sup>[25,31]</sup> We also applied the Pd-based electrocatalysts to the HER (Figures S11 and S12, and Table S3, Supporting Information). The v-PdCuCo-AS shows the better HER activity than PdCu-AS and commercial Pd/C, which further evidents the beneficial effects of the surface vacancies.<sup>[6]</sup>

The accelerated degradation tests (ADT) of the v-PdCuCo-AS catalyst was tested in  $0.1 \text{ M HClO}_4$  solution at the potential between 0.6 and 1.1 V (vs RHE). Figure S13 in the Supporting Information shows the electrocatalytic durability of high-performance PdCu-AS and v-PdCuCo-AS catalysts. The CVs, ORR polarization curves, and the corresponding Tafel plots (Figure S13) of the v-PdCuCo-AS catalyst before and after 4000 cycles between 0.6 and 1.1 V (vs. RHE) all suggest good stability of the v-PdCuCo-AS. These results suggest good stability of the v-PdCuCo-AS. There is 13.36% loss of MA for the PdCu-AS at 0.9 V versus RHE after 4000 cycles, while only 0.26% loss of MA for the v-PdCuCo-AS under the same condition (Figure S14, Supporting Information), revealing that the superior catalytic durability of the v-PdCuCo-AS catalyst. The catalytic performance variation between the PdCu-AS and v-PdCuCo-AS is likely to be caused by the synergistic effect of correlated defects and doped Co atoms. The compressive surface strain of the v-PdCuCo-AS protected the interior Pd atoms from losing by the place-exchange mechanism during the ADT. In addition, the self-supporting property of the special AS structure can improve the electrocatalysis stability of the v-PdCuCo-AS (Figures S13 and S14, Supporting Information).<sup>[13,40]</sup> The structures of the v-PdCuCo-AS catalysts before and after ADT were characterized by HRTEM (Figure S15, Supporting Information), showing negligible change of the structure.

The ORR polarization of the catalysts was also tested in  $\text{O}_2$ -saturated  $0.1 \text{ M KOH}$  solution as shown in Figure S16 in the Supporting Information. The half-wave potentials of the v-PdCuCo-AS is 0.901 V, which is  $\approx 37 \text{ mV}$  larger than that of PdCu-AS (0.864 V), suggesting its decreased ORR overpotential.<sup>[29]</sup> The corresponding Tafel plots inserted in Figure S16A in the Supporting Information further indicate the enhanced activity. At 0.8 V versus RHE, the MA of the v-PdCuCo-AS is  $0.21 \text{ A mg}^{-1}$ , 1.63 times of PdCu-AS. Similar behavior is also observed at 0.9 V. The MA of the v-PdCuCo-AS is 1.68 times larger than that of PdCu-AS. The v-PdCuCo-AS reported herein also show excellent catalytic performance toward alcohol oxidation in half cells, such as methanol oxidation reaction (MOR) and ethanol oxidation reaction (EOR). As shown in Figure S16C,D in the Supporting Information, the v-PdCuCo-AS exhibits better MOR activity and shows 2.21 times MOR MA ( $0.17 \text{ A per mgPd}$ ) than PdCu-AS. For EOR, the MA of v-PdCuCo-AS is  $0.823 \text{ A per mgPd}$  (Figure S16E,F, Supporting Information), 2.44 times higher than that of the PdCu-AS. Furthermore, the two typical current peak ratios for the MOR and EOR, one on the forward (If) and the other on the reverse potential scan (Ib), can act as the preliminary evaluation for the antipoisoning ability.<sup>[7,13]</sup> The ratio of If/Ib of the v-PdCuCo-AS for EOR is higher than that of PdCu-AS. Figure S17 in the

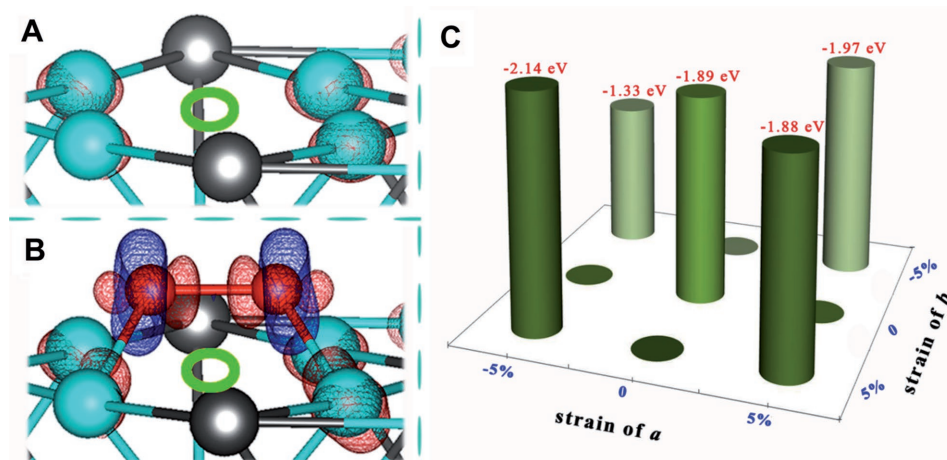


**Figure 4.** The deformation charge density of A) the vacancy in v-PdCuCo-AS and B) O<sub>2</sub> adsorbed v-PdCuCo-AS, and C) the adsorption energies of O<sub>2</sub> on strained v-PdCuCo-AS species (green ring: vacancy, light blue ball: Cu atom, and black ball: Pd atom) (blue area: charge accumulation and red area: charge depletion).

Supporting Information shows the anodic portions of the CV corresponding to the CO oxidation process for the PdCu-AS and v-PdCuCo-AS. The onset potential of CO-stripping on v-PdCuCo-AS shifts more negatively than that on PdCu-AS, which further indicated that the v-PdCuCo-AS have a higher durability against CO poison than PdCu-AS.<sup>[52]</sup> The potential-dependent steady-state current curves (recorded at 3000 s) of EOR pointing toward the same trend is shown in Figure S18 in the Supporting Information. The v-PdCuCo-AS for MOR exhibits inferior stability in the initial test, while conserves stability without obvious decay during subsequent tests. Apparently, v-PdCuCo-AS shows more superior stability compared to PdCu-AS. These results reveal that the catalysts with vacancies have better performance for MOR and EOR than the corresponding counterparts as illustrated in Tables S4 and S5 in the Supporting Information.

As widely accepted, modifying the electronic structure of the electrocatalysts through the control of defects is an intrinsic regulatory approach to improve its catalytic performance.<sup>[4]</sup> For this system, the vacancies on the exterior surfaces of the catalyst play an important role in promoting the ORR performance of the v-PdCuCo-AS. To gain further insight on the relationship between the vacancies and ORR performance of the PdCuCo-AS, DFT calculations were performed to explore electronic structures of catalysts and their influence on catalytic properties. Clearly, the electrons are redistributed around the vacancy on the surface of v-PdCuCo-AS, as shown in Figure 4A. Although the O<sub>2</sub> can maintain its construction above vacancy, but the bond distance of O<sub>2</sub> is expanded from 1.21 to 1.43 Å. These phenomena can be reasonably explained according to the charge transfer. As displayed in Figure 4B, some charge accumulation around O atoms and charge depletion areas in red colors can be found around Pd atoms, which means that the charge transferred from Pd atoms to O atoms, resulting in the ionization of O<sub>2</sub>. The ionized O<sub>2</sub> can further enhance the performance of ORR, in consistent with our experiment descriptions. Significantly, there is unobvious electron transfer from Cu to O<sub>2</sub>, which means that the influence of Cu is limited in ORR. It has been experimentally demonstrated that the lattice of PdCu-AS

is expanded for Co-embedding, and the influence of lattice change also calculated by DFT. The adsorption energies for O<sub>2</sub> are increased with the change of lattice (Figure 4C), which again demonstrates that the vacancy structure can enhance the performance of ORR.

The v-PdCuCo-AS reported here shows excellent electrochemical activity toward ORR. Owing to the vacancies sites on the exterior surface and the Co-embedded, the polarized electronic structures of the v-PdCuCo-AS can effectively promote the charge transfer in the processes of ORR. The MA toward the ORR (at 0.9 V vs RHE) is found to be 15.55 times that of a commercial Pd/C catalyst and 3.34 times that of the PdCu-AS (0.053 A mg<sup>-1</sup>), respectively. In the case of high surface-to-volume ratio AS, the v-PdCuCo-AS not only exhibits substantial enhancement in mass activity toward ORR, but also retains better durability. Together, our studies show an attractive strategy by engineering the surface structure of the Pd-based-AS nanocatalysts, which are possible to achieve a randomly scattered distribution of vacancy defects on the surface of the catalysts.

## Experimental Section

**Chemicals and Materials:** Hexadecyltrimethylammonium bromide (CTAB, 99%) and Pd/C (20% Pd) were purchased from Sigma-Aldrich. Sodium tetrachloropalladate (II), potassium bromide, ascorbic acid, copper (II) nitrate trihydrate and perchloric acid (HClO<sub>4</sub>, 70%) were supplied by Sinopharm Chemical Reagent Co., Ltd. All the chemicals were of analytical reagent and the ultrapure water in this experiment was with a conductivity of 18.25 MΩ cm.

**Preparation of PdCu-AS:** 6 mg Na<sub>2</sub>PdCl<sub>4</sub>, 1.62 mg Cu(NO<sub>3</sub>)<sub>2</sub>, 50 mg KBr, 100 mg CTAB, and 90 mg ascorbic acid were added in sequence into a reaction bottle with 5 mL H<sub>2</sub>O at 30 °C under constant magnetic stirring until the mixture well blended. Nitrogen was blown through the bottle to remove oxygen from the system. To obtain well-defined PdCu-AS catalyst, the system was heated up to 90 °C and kept for 90 min under the blow of nitrogen. After centrifugation/wash with ethanol, the final products were obtained.

**Synthesis of v-PdCuCo-AS:** 6 mg Na<sub>2</sub>PdCl<sub>4</sub>, 1.62 mg Cu(NO<sub>3</sub>)<sub>2</sub>, 50 mg KBr, 100 mg CTAB, 90 mg ascorbic acid, and 0.351 mg Co(NO<sub>3</sub>)<sub>2</sub> were

added in sequence into a reaction bottle with 5 mL H<sub>2</sub>O at 30 °C under constant magnetic stirring until the mixture well blended. To obtain well-defined v-PdCuCo-AS catalyst, the system was heated up to 90 °C and kept for 120 min to remove the Co atoms under the blow of nitrogen. After a centrifugation/wash cycle, the v-PdCuCo-AS catalysts were obtained.

**Structural and Compositional Analyses:** High-angle annular dark-field scanning TEM (HAADF-STEM) and energy dispersive X-ray (EDX) mapping analyses were performed using a JEM-ARM200F (JEOL) with an aberration corrector operated at 200 kV. The high-resolution transmission electron microscopy (HRTEM) measurements were conducted on a JEM-2010FEF at an accelerating voltage of 200 kV. Low-magnification TEM measurements were made on a HITACHI H-7650 transmission electron microscope at an acceleration voltage of 80 kV. The compositions of the Pd-based catalysts were determined by ICP-MS (NexION 300Q, PerkinElmer). The XRD analysis was carried out on a Bruker D8 Advance X-ray diffractometer with Cu K<sub>α</sub> radiation. The XPS analysis was measured by a Thermo VG Multilab 2000 spectrometer with a monochromatic Al K<sub>α</sub> radiation source at room temperature. The XAFS experiments and data processing were performed at the 4W1A-X in Beijing Synchrotron Radiation Facility. The data fitting was done by Artemis program in IFFEFIT.

**Electrocatalytic Measurements:** The ORR tests were carried out in 0.1 M HClO<sub>4</sub> at room temperature through the Pine electrochemistry station using a glassy-carbon rotating disk electrode (diameter: 5 mm, area: 0.196 cm<sup>2</sup>) as the working electrode to load a thin catalyst film. The intact Ag/AgCl (3 M KCl) was used as reference electrode and a Pt nanowire was the counter electrode. The concentrations of metal Pd were measured by ICP-MS and the loading amounts of Pd for v-PdCuCo-AS and PdCu-AS, and the commercial Pd/C (JM) catalysts were calculated as 0.046, 0.059, and 0.15 mg Pd cm<sup>-2</sup>, respectively. The ECSAs of the catalysts were determined by integrating the hydrogen adsorption charge on CVs, which tested in N<sub>2</sub>-saturated 0.1 M HClO<sub>4</sub> solution with the scan rate of 50 mV s<sup>-1</sup>. The ORR tests were conducted in O<sub>2</sub>-saturated 0.1 M HClO<sub>4</sub> with the scan and rotation rates of 10 mV s<sup>-1</sup> and 1600 rpm, respectively. The accelerated durability tests (ADTs) for the catalysts were performed in 0.1 M HClO<sub>4</sub> with the sweeping potential from 0.6 to 1.1 V versus RHE at a sweep rate of 0.1 V s<sup>-1</sup> for 4000 cycles. The ORR tests in alkaline were performed at room temperature in 0.1 M KOH with the same scan and rotation rates. The MOR and EOR measurements were conducted in 1 M KOH + 1 M CH<sub>3</sub>OH or 1 M KOH + 1 M CH<sub>3</sub>CH<sub>2</sub>OH solution at room temperature. The scan rate for MOR and EOR tests was at 50 mV s<sup>-1</sup>. The chronoamperometry was employed to investigate the stability of the catalysts. For HER, all the electrochemical measurements were performed in a three-electrode system in 0.5 M H<sub>2</sub>SO<sub>4</sub> electrolyte. To prepare the working electrode, the catalysts were incorporated onto carbon black (Vulcan XC-72) and dispersed ultrasonically in Nafion (0.05 wt%) isopropyl alcohol solution to form an ink. The compositions of the ink were determined by ICP-optical emission spectroscopy. Then the ink was pipetted onto a GCE as a working electrode and the graphite rod was chosen as the counter electrode. The loading amounts of the three catalysts were 10 μg cm<sup>-2</sup>.

**Calculation Methods:** It is well known that the chemical reaction sites are almost on materials surfaces. Therefore, surface models of PdCu-based structures (including PdCu and Co-doped PdCu) were built with a vacuum space of 15 Å. And based on these models, it was attempted to understand the relationship between the structure and ORR performance of the Co-PdCu by using DFT calculations. And in present work, all calculations were performed by using the Vienna ab initio simulation package.<sup>[53]</sup> The ion–electron interactions are described by the projected augmented wave method combined with exchange–correlation functional of Perdew–Burke–Ernzerhof within the generalized gradient approximation.<sup>[54,55]</sup> For each numerical convergence, the thresholds of 10<sup>-5</sup> eV in energy and 10<sup>-2</sup> eV Å<sup>-1</sup> in force under a considerable cutoff energy of 500 eV can be accepted. Grimme DFT-D2 dispersion correction method<sup>[56]</sup> was employed to describe the weak interactions of O<sub>2</sub> on models. The binding energies (E<sub>b</sub>) of O<sub>2</sub> on PdCu-based structures were obtained by the equation, E<sub>b</sub> = E<sub>Ad</sub> – E<sub>PdCu</sub> – E<sub>O<sub>2</sub></sub>,

where E<sub>Ad</sub>, E<sub>PdCu</sub>, and E<sub>O<sub>2</sub></sub> represent the total energies of O<sub>2</sub> adsorbed PdCu-based structures, PdCu-based structures, and O<sub>2</sub>, respectively. The deformation charge density (ρ<sub>d</sub>) describes the charge difference between atoms and compounds, and it was calculated by ρ<sub>d</sub> = ρ<sub>scf</sub> – ρ<sub>atom</sub>, where ρ<sub>scf</sub> and ρ<sub>atom</sub> are the charge density of selected compound and the charge densities of all atoms in whole system, respectively, which are performed by VESTA code.<sup>[57]</sup>

## Supporting Information

Supporting Information is available from the Wiley Online Library or from the author.

## Acknowledgements

Y.Z. and D.R. contributed equally to this work. The syntheses were supported by the National Key R & D Program (2016YFD0500706), the National Natural Science Foundation of China (21375043, 21778020), the Sci-tech Innovation Foundation of Huazhong Agriculture University (2662017PY042), the Research Grant Council of Hong Kong (Grant Number: PolyU 152145/15E), Hong Kong Polytechnic University (Grant Numbers: G-SB53, 1-ZVGH) and the Natural Science Foundation of Jiangsu Province (Grant Numbers: BK20140526).

## Conflict of Interest

The authors declare no conflict of interest.

## Keywords

compressive strain, enhanced electrochemical performance, exterior atomic vacancy, oxygen reduction reaction, PdCuCo alloys

Received: July 25, 2017

Revised: September 21, 2017

Published online:

- [1] H. A. Gasteiger, S. S. Kocha, B. Sompalli, F. T. Wagner, *Appl. Catal., B* **2005**, *56*, 9.
- [2] M. K. Debe, *Nature* **2012**, *486*, 43.
- [3] T. H. Wesley, R. Marcel, A. S. Kelsey, G. Alexis, S. Jin, S. H. Yang, *Energy Environ. Sci.* **2015**, *8*, 1404.
- [4] D. Yan, Y. Li, J. Huo, R. Chen, L. Dai, S. Wang, *Adv. Mater.* **2017**, *1606459*, 1.
- [5] J. Staszak-Jirkovský, C.-D. Malliakas, P.-P. Lopes, N. Danilovic, S.-S. Kota, K.-C. Chang, B. Genorio, D. Strmcnik, V.-R. Stamenkovic, M.-G. Kanatzidis, N.-M. Markovic, *Nat. Mater.* **2016**, *15*, 197.
- [6] C. Chen, Y. Kang, Z. Huo, Z. Zhu, W. Huang, H. Xin, J. Snyder, D. Li, J. Herron, M. Mavrikakis, M. Chi, K. L. More, Y. D. Li, N. M. Markovic, G. A. Somorjai, P. D. Yang, V. R. Stamenkovic, *Science* **2014**, *343*, 1339.
- [7] Y. Zuo, K. Cai, L. Wu, T. Li, Z. Lv, H. Han, *J. Mater. Chem. A* **2015**, *3*, 1388.
- [8] G. J. Leong, M. C. Schulze, M. B. Strand, D. Maloney, *Appl. Organomet. Chem.* **2014**, *28*, 1.
- [9] Y. Xia, *Angew. Chem., Int. Ed.* **2009**, *48*, 60.
- [10] R. A. Martinez-Rodriguez, F. J. Vidal-Iglesias, J. Solla-Gullon, C. R. Cabrera, J. M. Feliu, *J. Am. Chem. Soc.* **2014**, *136*, 1280.
- [11] M. Gong, G. Fu, T. Lu, *ACS Appl. Mater. Interfaces* **2014**, *6*, 7301.

- [12] Y. Wang, S. Choi, X. Zhao, S. Xie, H. Peng, M. Chi, C. Huang, Y. Xia, *Adv. Funct. Mater.* **2014**, *24*, 131.
- [13] K. Jiang, P. Wang, S. Guo, X. Zhang, X. Shen, G. Lu, D. Su, X. Huang, *Angew. Chem., Int. Ed.* **2016**, *55*, 1.
- [14] S. Gao, Y. Lin, X. Jiao, Y. Sun, Q. Luo, W. Zhang, D. Li, J. Yang, Y. Xie, *Nature* **2016**, *529*, 68.
- [15] J. Xie, H. Zhang, S. Li, R. Wang, X. Sun, M. Zhou, J. Zhou, X. W. Lou, Y. Xie, *Adv. Mater.* **2013**, *25*, 5807.
- [16] F. Cheng, J. Shen, B. Peng, Y. Pan, Z. Tao, J. Chen, *Nat. Chem.* **2011**, *3*, 79.
- [17] A. Shen, Y. Zou, Q. Wang, R. A. Dryfe, X. Huang, S. Dou, L. Dai, S. Wang, *Angew. Chem., Int. Ed.* **2014**, *53*, 10804.
- [18] H. Li, C. Tsai, A. L. Koh, L. Cai, A. W. Contryman, A. H. Fragapane, J. Zhao, H. Han, H. C. Manoharan, F. Abild-Pedersen, J. K. Nørskov, X. Zheng, *Nat. Mater.* **2016**, *15*, 48.
- [19] L. Dai, Y. Xue, L. Qu, H. J. Choi, J. B. Baek, *Chem. Rev.* **2015**, *115*, 4823.
- [20] Y. Nie, L. Li, Z. Wei, *Chem. Soc. Rev.* **2015**, *44*, 2168.
- [21] X. Huang, Z. Zhao, L. Cao, Y. Chen, E. Zhu, Z. Lin, M. Li, A. Yan, A. Zettl, M. Wang, X. Duan, T. Mueller, Y. Huang, *Science* **2015**, *348*, 1230.
- [22] Y. Wang, N. Zhao, B. Fang, H. Li, X. Bi, H. Wang, *Chem. Rev.* **2015**, *115*, 3433.
- [23] M. Shao, Q. Chang, J. P. Dodelet, R. Chenitz, *Chem. Rev.* **2016**, *116*, 3594.
- [24] S. Bai, Q. Shao, P. Wang, Q. Dai, X. Wang, X. Huang, *J. Am. Chem. Soc.* **2017**, *139*, 6827.
- [25] J. Liu, K. He, W. Wu, T. Song, M.-G. Kanatzidis, *J. Am. Chem. Soc.* **2017**, *139*, 2900.
- [26] S. Ma, H. Li, B. Hu, X. Cheng, Q. Fu, S. Yu, *J. Am. Chem. Soc.* **2017**, *139*, 5890.
- [27] H. Li, Q. Fu, L. Xu, S. Ma, Y. Zheng, X. Liu, S. Yu, *Energy Environ. Sci.* **2017**, *10*, 1751.
- [28] H. Wang, S. Xu, C. Tsai, Y. Li, C. Liu, J. Zhao, Y. Liu, H. Yuan, F. Abild-Pedersen, F. B. Prinz, J. K. Nørskov, Y. Cui, *Science* **2016**, *354*, 1031.
- [29] L. Bu, N. Zhang, S. Guo, X. Zhang, J. Li, J. Yao, T. Wu, G. Lu, J. Ma, D. Su, X. Huang, *Science* **2016**, *354*, 1410.
- [30] Y. Zuo, L. Wu, K. Cai, T. Li, W. Yin, D. Li, N. Li, J. Liu, H. Han, *ACS Appl. Mater. Interfaces* **2015**, *7*, 17725.
- [31] E. Ye, M.-D. Regulacio, S.-Y. Zhang, X. Jun, M.-Y. Han, *Chem. Soc. Rev.* **2015**, *44*, 6001.
- [32] Z. Fan, H. Zhang, *Chem. Soc. Rev.* **2016**, *45*, 63.
- [33] W. Chen, R. Yu, L. Li, A. Wang, Q. Peng, Y. Li, *Angew. Chem., Int. Ed.* **2010**, *49*, 2917.
- [34] C. Xu, Y. Liu, J. Wang, H. Geng, H. Qiu, *J. Power Sources* **2012**, *199*, 124.
- [35] C. Xu, A. Liu, H. Qiu, Y. Liu, *Electrochem. Commun.* **2011**, *13*, 766.
- [36] D. Wang, H. L. Xin, H. Wang, Y. Yu, E. Rus, D. Muller, F. J. DiSalvo, H. D. Abruña, *Chem. Mater.* **2012**, *24*, 2274.
- [37] Y. Wu, C. Wang, L. Zou, Q. Huang, H. Yang, *J. Electroanal. Chem.* **2017**, *789*, 167.
- [38] F. Zhu, M. Wang, Y. He, G. Ma, Z. Zhang, X. Wang, *Electrochim. Acta* **2014**, *148*, 291.
- [39] M. Jiang, W. Liu, X. Yang, Z. Jiang, T. Yao, S. Wei, X. Peng, *ACS Nano* **2015**, *9*, 10950.
- [40] M. Li, Z. Zhao, T. Cheng, A. Fortunelli, C. Chen, R. Yu, Q. Zhang, L. Gu, B. V. Merinov, Z. Lin, E. Zhu, T. Yu, Q. Jia, J. Guo, L. Zhang, W. A. Goddard III, Y. Huang, X. Duan, *Science* **2016**, *354*, 1414.
- [41] H. Wang, S. Xu, C. Tsai, Y. Li, C. Liu, J. Zhao, Y. Liu, H. Yuan, F. Abild-Pedersen, F. B. Prinz, J. K. Nørskov, Y. Cui, *Science* **2016**, *354*, 1031.
- [42] X. Xia, Y. Wang, A. Ruditskiy, Y. Xia, *Adv. Mater.* **2013**, *25*, 6313.
- [43] Z. Peng, H. Yang, *Nano Today* **2009**, *4*, 143.
- [44] Y. Xiong, H. Cai, B.-J. Wiley, J. Wang, M.-J. Kim, Y. Xia, *J. Am. Chem. Soc.* **2007**, *129*, 3665.
- [45] Y. Xia, X. Xia, H.-C. Peng, *J. Am. Chem. Soc.* **2015**, *137*, 7947.
- [46] Y. Xiong, Y. Xia, *Adv. Mater.* **2007**, *19*, 3385.
- [47] Y. Zuo, T. Li, D. Rao, X. Lei, Q. Li, G. Zhu, R. Lu, H. Han, *J. Phys. Chem. C* **2016**, *120*, 12305.
- [48] G. Wang, B. Huang, L. Xiao, Z. Ren, H. Chen, D. Wang, J. Lu, H. D. Abruña, L. Zhuang, *J. Am. Chem. Soc.* **2014**, *136*, 9643.
- [49] L. Ma, C. Wang, M. Gong, L. Liao, R. Long, J. Wang, D. Wu, W. Zhong, M. J. Kim, Y. Chen, Y. Xie, Y. Xiong, *ACS Nano* **2012**, *6*, 9797.
- [50] Y. Zuo, T. Li, H. Ren, G. Zhu, K. Han, L. Zhuang, H. Han, *J. Mater. Chem. A* **2016**, *4*, 15169.
- [51] J. Hong, Y. Kim, D.-H. Wi, S. Lee, S.-U. Lee, Y.-W. Lee, S. Choi, S.-W. Han, *Angew. Chem., Int. Ed.* **2016**, *55*, 2753.
- [52] S. J. Lee, S. Mukerjee, E. Ticianelli, J. McBreen, *Electrochim. Acta* **1999**, *44*, 3283.
- [53] G. Kresse, J. Furthmüller, *Phys. Rev. B* **1996**, *54*, 11169.
- [54] P. Blöchl, *Phys. Rev. B* **1994**, *50*, 17953.
- [55] G. Kresse, D. Joubert, *Phys. Rev. B* **1999**, *59*, 1758.
- [56] G. Stefan, *J. Comput. Chem.* **2006**, *27*, 1787.
- [57] M. Koichi, F. Izumi, *J. Appl. Crystallogr.* **2011**, *44*, 1272.